We are IntechOpen, the world's leading publisher of Open Access books
Built by scientists, for scientists

4,800
Open access books available

122,000
International authors and editors

135M
Downloads

154
Countries delivered to

Our authors are among the

TOP 1%
most cited scientists

12.2%
Contributors from top 500 universities

CLARIVATE ANALYTICS

BOOK CITATION INDEX

INDEXED

WEB OF SCIENCE™

Selection of our books indexed in the Book Citation Index
in Web of Science™ Core Collection (BKCI)

Interested in publishing with us?
Contact book.department@intechopen.com

Numbers displayed above are based on latest data collected.
For more information visit www.intechopen.com

Ultra-Fast All-Optical Memory based on Quantum Dot Semiconductor Optical Amplifiers (QD-SOA)

Yossef Ben Ezra and Boris I. Lembrikov

Additional information is available at the end of the chapter

Abstract

All-optical signal processing is characterized by high bit-rate, power efficiency, high bandwidth, and transparency. All-optical logic gates are basic logic units for the all-optical signal processing implementation. Typically, all-optical gates are based on strong optical nonlinearities related in particular to semiconductor optical amplifiers (SOA). We briefly review the state of art in the field of all-optical logic gates and all-optical memory. In the original part, we discuss the ultrafast all-optical memory loop based on the Mach-Zehnder interferometer (MZI) with quantum dot (QD) semiconductor optical amplifier (SOA) in each arm.

Keywords: all-optical signal processing, quantum dots (QD), semiconductor optical amplifier (SOA)

1. Introduction

Optical signal processing is based on the using of linear and nonlinear optical techniques in order to manipulate and process digital, analogue, and quantum information [1]. Optical signal processing increases the processing speed of devices and reduces the energy consumption and latency of communication systems [1]. In particular, ultrafast optical nonlinearities provide a substantial speed advantage as compared to electronic techniques for simple logic: switching, regeneration, wavelength conversion (WC), performance monitoring, and analog-to-digital conversion (ADC) [1]. Silicon photonics and highly nonlinear nanophotonic devices are providing strong optical nonlinearities for ultrafast processing on millimeter length scales [1].

The recent progress in optical signal processing is based on the combination of the advanced modulation techniques, coherent detection, and digital signal processing (DSP) [2]. The

interface of all-optical techniques and advanced DSP will enhance electronic processing capabilities [1]. Optical signal processing is essentially based on the following advanced technologies: coherent detection, high-speed electronics for DSP, advances in strongly nonlinear materials and devices, photonic integrated circuits (PIC), and access to four optical domains of amplitude, phase, polarization, and wavelength [2]. A simple digital modulation scheme is the on-off keying (OOK) referred to as intensity modulation with direct detection (IM/DD) [3]. In such a case, an electrical binary bit stream modulates the intensity of an optical carrier inside the optical transmitter, and the resulting optical signal is converted to the original signal in the electrical domain in an optical receiver [4]. The phase modulation combined with the coherent detection increases the spectral efficiency (SE) of optical communication systems and improves the sensitivity of optical receivers [4]. In general case, amplitude-shift keying (ASK), phase-shift keying (PSK) or M-ary quadrature amplitude modulation (QAM) can be realized [3, 4]. Polarization-division multiplexing (PDM), advanced multilevel modulation formats such as M-ary QAM, digital spectral shaping at the transmitter, coherent detection and advanced forward error correction (FEC) can increase SE of the communication system [1]. Typically, DSP must overcome deterministic signal distortions, while FEC overcomes stochastic impairments caused by noise and interference [1]. At the transmitter, DSP together with digital-to-analog converters (DAC) and FEC converts the incoming data bits into a set of analogue signals [1]. An optical coherent receiver recovers the amplitude and phase of the signal by mixing it with the local oscillator (LO) which is typically a continuous-wave (CW) laser [3, 4]. DSP, ADC, and FEC recover the data from the set of analogue electrical signals [1]. The main functions of the receiver-based DSP are equalization and synchronization [1]. Equalization must realize the polarization rotation tracking and dispersion compensation including both the chromatic dispersion and polarization-mode dispersion (PMD) [1]. Synchronization carries out the transmitter and receiver electrical and optical signal frequency and phase matching [1].

The all-optical signal processing is implemented by using the nonlinear optical phenomena such as self-phase modulation (SPM), cross-phase modulation (XPM), four-wave mixing (FWM) related to the third-order susceptibility and sum frequency, difference frequency, second harmonic generation (SHG) related the second-order susceptibility [1–4]. The typical nonlinear elements used in optical communication systems are highly nonlinear optical fibers (HNLF), silicon waveguides, chalcogenide waveguides, photonic crystals, nonlinear optical loop mirrors (NOLM), parametric amplifiers, and semiconductor optical amplifiers (SOA) [2, 3]. SOA are characterized by the extremely strong third-order optical nonlinearity and fast response and can be integrated monolithically with other devices on the same chip [3].

Optically assisted signal processing combines optics and electronics for what each one of them does best [2]. Optical components can perform some functions very fast, while electronic components carry out complex computations with buffers and memory [2]. For instance, optically assisted network routing technique uses optical correlation on headers of Internet data packets [2]. Optically assisted signal processing can be also used for a target pattern search in large amounts of data [2]. In such cases, the data information is encoded on an optical carrier at Tb/s speed and sent to an optical correlator for pattern recognition [2]. The output at Gb/s speed is searched and processed electronically with high accuracy before being sent to the user [2].

In optical networks, the bandwidth mismatch between optical transmission and electronic routers results in the development of different optical signal processing and the investigation of optical packet switching (OPS) [5]. Some applications require selective switching of one or more bits to a different port [3]. The packet switching takes place when a packet of tens or hundreds of bits is selected from a bit stream [3]. The flip-flop memory is an essential component of the packet switch [3]. Typically, such a memory is implemented using two coupled lasers switching the output signal between two wavelengths λ_1 and λ_2 [3]. Recently, we proposed a novel architecture of an all-optical memory loop combining the ultrafast all-optical signal processor based on the Mach-Zehnder interferometer (MZI) with quantum dot (QD) SOA and the DSP block for the mitigation of dispersion and nonlinearity impairments [6].

The chapter is organized as follows. OPS in optical communication systems is discussed in Section 2. The different types of all-optical logic gates used in OPS are briefly reviewed in Section 3. The operation principle of the novel all-optical memory is described in Section 4. The QD SOA theoretical model is briefly discussed in Section 5. The numerical simulation results and conclusions are presented in Sections 6 and 7, respectively.

2. Optical packet switching (OPS)

OPS process requires many components for buffering, header processing, and switching [3]. Each packet begins with a header containing the destination information [3]. When a packet arrives at a node, a router reads the header and sends it toward its destination [3]. The basic element of an optical router is a packet switch directing incoming packets to the corresponding output ports depending on the information in the header [3].

Consider the architecture and operation principle of the all-optical packet switch. The scheme of the 1 × 2 all-optical packet switch is shown in **Figure 1** [3, 5, 7]. The all-optical packet switch consists of three functional blocks: the all-optical header-processing block, the all-optical flip-flop memory block, and the WC block [7]. All-optical header processing can be realized by using the different methods such as tunable Bragg gratings, FWM in a SOA, terahertz optical asymmetric demultiplexers (TOAD), two-pulse correlation in a semiconductor laser amplifier in a loop optical mirror (SLALOM) [5, 7].
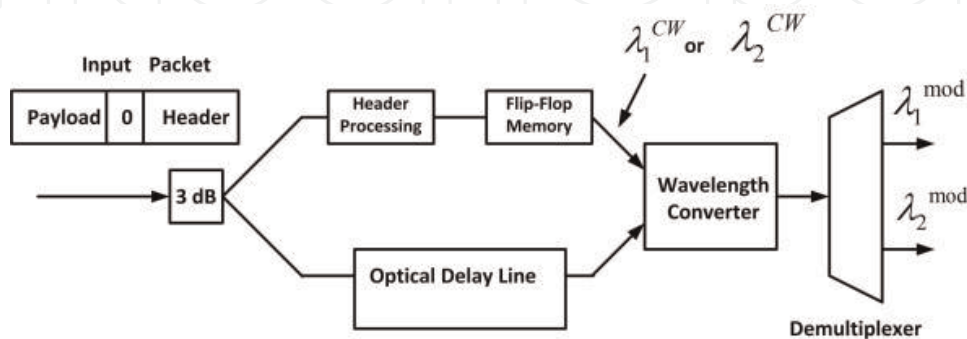
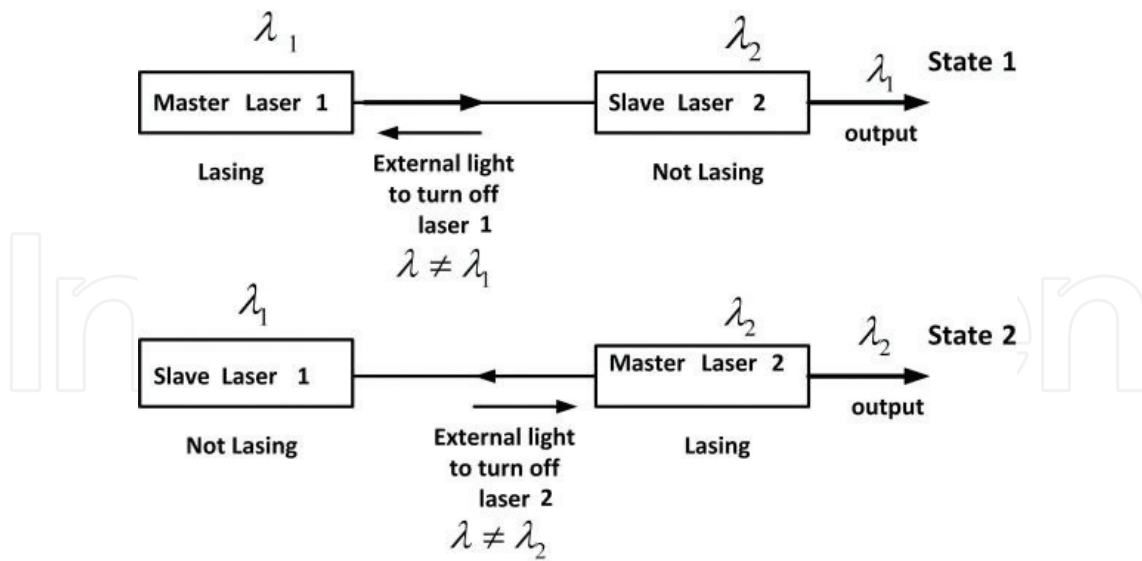**Figure 1.** System concept for 1 × 2 all-optical packet switches.

Figure 2. The all-optical flip-flop memory based on two coupled lasers.

The high-speed memory is necessary for OPS networks in order to avoid the packet collisions during packet routing [8]. The all-optical flip-flop memory is based on two coupled lasers with separate laser cavities and can have two states [7]. It is shown in **Figure 2** [7].

In state 1, light from laser 1 suppresses lasing in laser 2 emitting CW light at wavelength λ_1, while in state 2, light from laser 2 suppresses lasing in laser 1 emitting CW light at wavelength λ_2 [7]. The output pulse of the optical header processor is used to set the optical flip-flop memory into the desired wavelength [7]. The amount of light P_{sw} which is necessary for the change of states, the threshold carrier number N_{th}, and photon lifetime τ_p are given by, respectively [7]:

$$P_{sw} = E \frac{v_g R \tau_p}{L(1-R)} \ln\left(\frac{1}{R}\right)\left(1 - \frac{2R}{\delta(1-R)}\right)\left(\frac{I}{q} - \frac{N_{th}}{\tau_e}\right) \tag{1}$$

$$N_{th} = \frac{V}{\tau_p \Gamma v_g a} + N_0; \frac{1}{\tau_p} = v_g\left(\alpha_{\text{int}} + \frac{1}{L}\ln\left(\frac{1}{R}\right)\right) \tag{2}$$

Here, E is the photon energy, R is the reflectivity at the end facets of lasers, δ is the coupling constant between the two laser cavities, v_g is the group light velocity, L is the length of the active region in the laser, I is the injection current, q is the electron charge, τ_e is the carrier lifetime, V is the volume of the laser cavity active region, Γ is the confinement factor, a is the gain factor, N_0 is the carrier number at transparency, and α_{int} is the internal laser cavity losses factor. Note that the outputs of the lasers on the left side are defined by the reflectivity at the end facets of lasers R and do not influence the memory states.

WC component converts the incoming data packet wavelength to the output wavelength of the flip-flop memory [3]. The demultiplexer directs output at different wavelengths to different ports depending on the header information [3].

3. All-optical logic gates with SOA

In this section, we briefly discuss the scheme and operation principle of all-optical gates which are core logic units for the all-optical signal processing system implementation [9]. All-optical gates may be divided into two groups: without SOA and with SOA [9]. The all-optical gates without SOA are based on the change in nonlinear refraction index in silica fiber [9]. The intensity-dependent refractive index of silica results in the following nonlinear optical effects: SPM, cross gain modulation (XGM), and FWM [2, 9]. The all-optical gates without SOA based on these nonlinear optical phenomena can be realized in the following configurations: dispersion shifted fiber/high nonlinear fiber (DSF/HNLF) configuration; waveguide configuration; circular configuration; optical channel-dropping (C/D) filter configuration; multilayer waveguide configuration; double heterostructure optical thyristor (DHOT) configuration; and acousto-optical tunable filter (AOTF) configuration [9]. The detailed description and comparison between non-SOA gates are presented in Ref. [9]. For instance, DSF/HNLF, waveguide, circular, and AOTF configurations are polarization sensitive; DSF/HNLF, waveguide, circular configurations are characterized by bad or moderate integration capacity [9].

On the other hand, the SOA-based devices are mainly polarization non-sensitive and possess compact integration capacity [9]. They are highly competitive due to the high nonlinearity, low switching power, wide gain bandwidth, and compact size [8]. Recently, novel two inputs optical logic gates (NOT, AND, OR and NOR) based on a traveling wave SOA (TW-SOA) operating at 40 Gb/s had been demonstrated [10].

The implementation of all-optical gates with SOA is based on the different interferometer techniques such as ultra-high nonlinear interferometer (UNI), Sagnac interferometer (SI), MZI, and delay interferometer (DI) [9]. In these techniques, the XPM-induced phase shift is used for optical switching [4]. Typically, a weak signal pulse is divided equally between two arms of the interferometer and is undergoing identical phase shift in each arm [4]. In such a case, it is transmitted through constructive interference [4]. Consider now the situation when a pump pulse at a different wavelength as compared to the signal pulse is injected into one arm of the interferometer. As a result, the signal phase in that arm would be changed due to XPM. If the XPM-induced phase shift is close to π, the signal pulse will not be transmitted due to the destructive interference at the interferometer output [4]. An intense pulse pump can switch the signal pulse through the XPM-induced phase shift [4].

In particular, all-optical gate based on SOA-MZI can be realized with the copropagating, counterpropagating, and copropagating push-pull configurations [9]. Copropagation MZI operates on the principle of phase change caused by the light propagating through the 3 dB coupler [9]. MZI copropagating gates consist of a symmetrical MZI with two SOA placed in the upper and lower arm of the interferometer [9]. Data and clock pulses of different wavelengths are inserted into SOA operated under the gain saturation condition, where the optical gain is distributed between wavelengths according to their relative photon densities [9]. The data are transferred in the clock pulse in the inverted form in both arms of MZI [9]. After passing through the first 3 dB coupler, the phase difference $\pi/2$ is created between the upper and lower arms of clock pulse, after passing through the second 3 dB coupler the total phase

shift becomes π [9]. Then, if both data have the same value, they will cancel, and at the T-port 0 will appear, if data have different value, then it will not cancel and 1 will appear at the T-port [9]. In MZI counter-propagating gates, the clock and data pulse propagate in opposite directions through MZI [9]. If any of the data is 1, then XPM between the clock and data pulse inside SOA creates the differential phase shift between the two clock components, MZI becomes unbalanced, and the clock pulse exits at T-port [9]. If both the data are the same, the total phase shift will become π, and the clock pulse is cancelled at T-port [9].

Consider now a typical all-optical logic element based on transforming of XPM into an intensity modulation and implemented as the MZI copropagating push-pull gate with SOA in the two arms shown in **Figure 3** [9]. The optical fibers are used as interconnects. The SOA-based MZI with couplers at the input and output is shown in **Figure 4**. At the SOA-based MZI block output, there is a coupler shown in **Figure 4**. The outputs at the right side of this coupler are connected to the T-port and R-port shown in **Figure 3**.

Note that the co-propagating data streams configuration permits to avoid the SOA length restriction, and the MZI with push-pull configuration allows increasing the memory bit-rate beyond the limitation of the SOA carrier recovery time [8]. The copropagating data streams A and B of the same wavelengths are inserted into upper and lower arm of MZI shown in **Figure 4**.

The data A in the upper arm is ahead of one bit period to data B traveling in the lower arm of MZI, and the lower arm data B is one bit period ahead to upper arm data A [9]. As a result, a
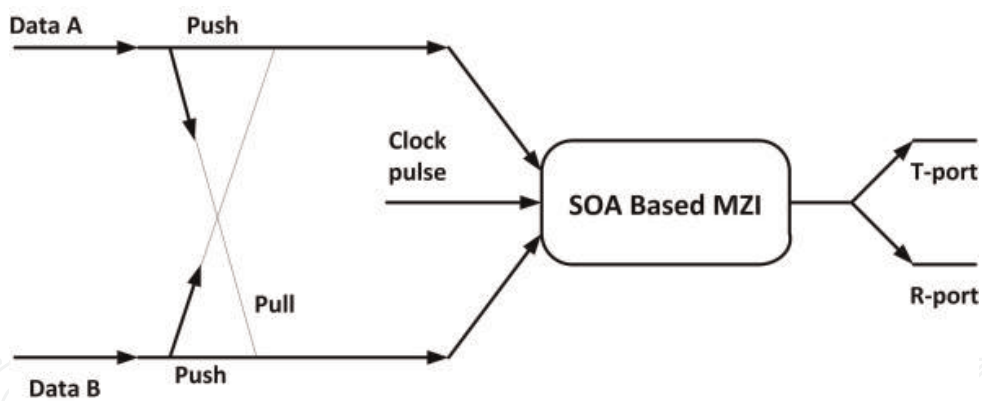

Figure 3. MZI with push-pull configuration.
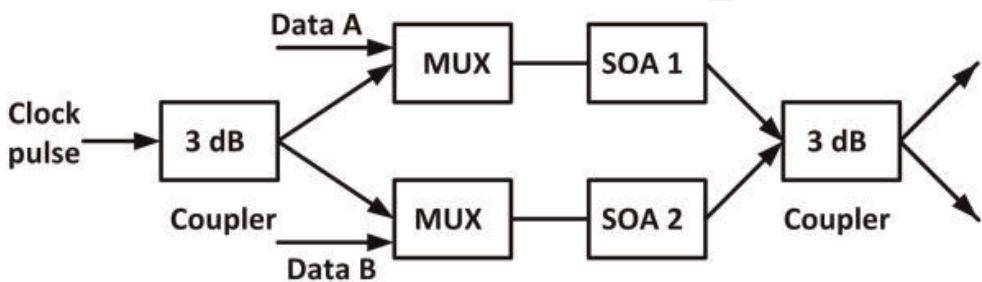

Figure 4. SOA–based MZI.

switching window for data streams occurs [9]. The clock pulse copropagating with the data streams A and B is inserted into the 3 dB coupler. Assume that the data A is 1 and data B is 0. Then, the pulse from data A splits into two parts in such a way that one pulse is pushed to the upper SOA 1 and other is delayed by the switching window. Consequently, the upper SOA 1 is switched before the lower SOA 2 [9]. The MZI is unbalanced, and clock wave is switched to the T-port. In the opposite case, when data A is 0 and data B is 1, then lower SOA 2 is switched and wave also appears at T-port [9]. Assume now that data A and data B are the same. As a result, SOA 1 and SOA 2 are equally influenced by the injected pulse. The respective push and pull pulse temporarily coincide with each other, the phase difference between the two arms of MZI equals to zero, and no switching occurs at T-port [9].

The disadvantages of the all-optical logic gates discussed above are twofold: (i) the operating speed of SOA is limited by the carrier recovery time of the order of magnitude of 100 ps; (ii) the scheme can be used only for OOK modulation format [8]. However, the SOA operation rate can be significantly increased up to 100 Gb/s by using the quantum dot semiconductor optical amplifiers (QD-SOA) [8, 11]. A theoretical model of an ultrafast all-optical signal processor based on QD-SOA MZI has been developed with limiting bit rates of 100 and 200 Gb/s at the injection currents of I = 30 mA and I = 50 mA, respectively [12].

4. All-optical memory loop based on SOA MZI

Consider now an all-optical memory loop consisting of an AND gate and a regenerator based on the two push-pull co-propagating MZI with a SOA in each arm and couplers at the input and the output shown in **Figure 4** and discussed in the previous section [8]. The scheme of the all-optical memory loop is shown in **Figure 5** [8]. The input data burst at the wavelength λ_2 is inserted into the memory through the AND gate is converted into the output data burst at the wavelength λ_1 [8]. A regenerator is used into the loop in order to improve the quality of the data burst at the wavelength λ_1 eliminating the signal degradation caused by dispersion, nonlinearity, and other physical impacts [8]. The output of the regenerator is fed back to the AND gate as a pump at the wavelength λ_3 [8]. The data can be stored in the loop for a long term [8]. The length of the data burst nT must be less than or equal to the length of the memory loop NT where T is the bit period [8].

The data format of the all-optical memory shown in **Figure 5** is OOK, while for the PSK modulation format the memory should be modified [8].

Recently, we proposed a novel architecture of an all-optical memory loop combining the ultrafast all-optical signal processor based on QD-SOA MZI [12] and the DSP block for the mitigation of the dispersion and nonlinearity impairments [6]. The proposed all-optical memory loop is shown in **Figure 6**. The advantages of the novel all-optical memory loop are following [6].

1. It includes only one MZI with two QD-SOA reducing the complexity of the electronic synchronization scheme.

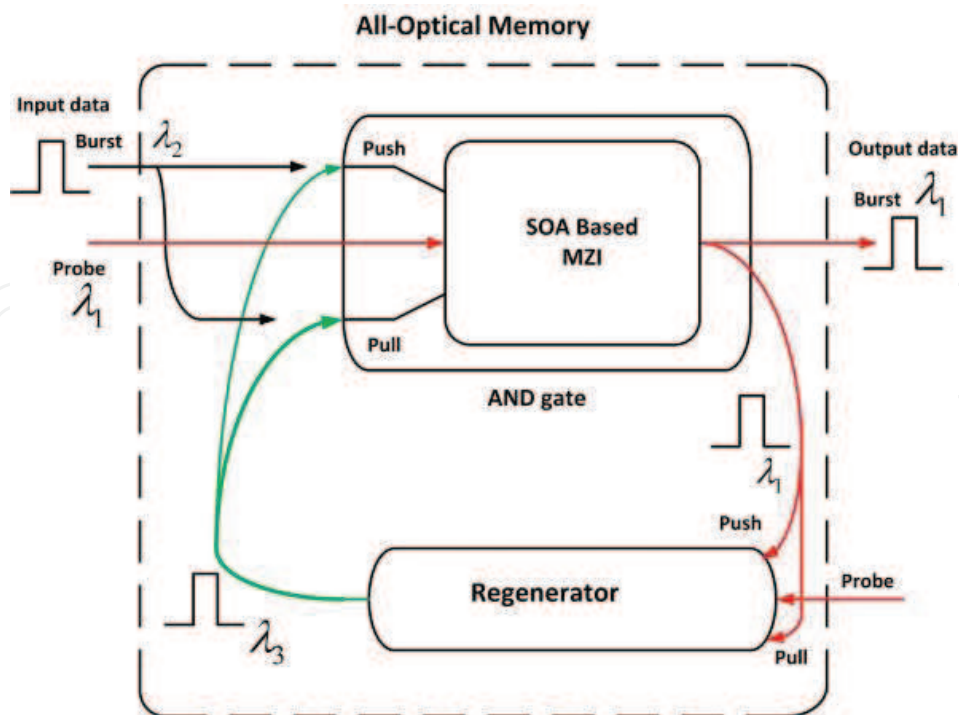2. It can operate at the bit rates up to 100 Gb/s due to the fast gain recovery time of QD-SOA.

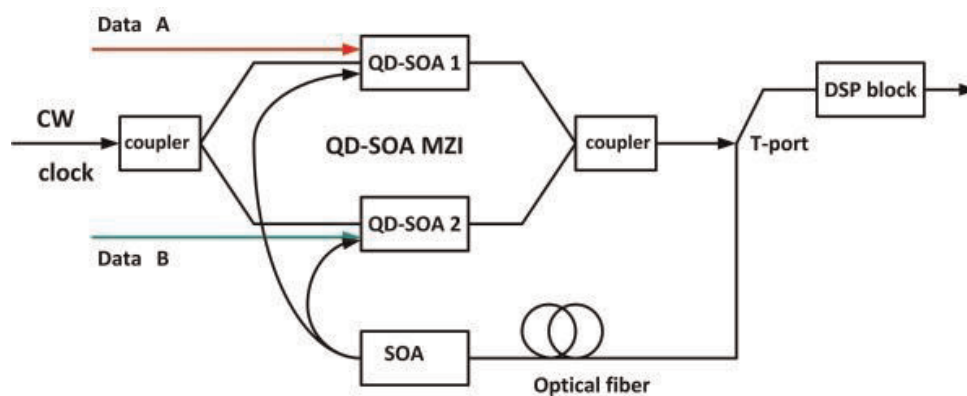**Figure 5.** Schematic setup of the all-optical memory based on SOA MZI.

Figure 6. The architecture of the all-optical memory loop based on QD-SOA–based MZI.

3. DSP block can improve the signal quality as compared to an MZI-based regenerator.

4. An additional SOA is inserted into the loop in order to compensate the optical fiber losses and to increase the loop length.

In our case, the phase difference at the output of the QD-SOA–based MZI is caused by the signal power difference in the upper and lower MZI arms, unlike the MZI copropagating push-pull gate mentioned above [9]. Typically, 80 and 20% of the input signal power were fed through the coupler into the upper and lower arm of the MZI, respectively [6]. As a result, dynamic processes in QD-SOA placed into the upper and lower arms of MZI are characterized by different carrier relaxation time and gain recovery time, and the flatness of the switching window is significantly improving [6].

The QD-SOA MZI output light intensity P_{out} and phase difference $\varnothing_1(t) - \varnothing_2(t)$ are given by Refs. [12–14]:

$$P_{out} = \frac{P_{in}}{4}\{G_1(t) + G_2(t) - 2\sqrt{G_1(t)G_2(t)}\cos[\phi_1(t) - \phi_2(t)]\} \tag{3}$$

$$\phi_1(t) - \phi_2(t) = -\frac{\alpha}{2}\ln\left(\frac{G_1(t)}{G_2(t)}\right) \tag{4}$$

where the P_{in} is continuous wave (CW) clock stream optical signal divided and introduced into the two QD-SOA, $G_{1,2} = exp(g_{1,2}L)$ and $\varnothing_{1,2}(t)$ are the gain and phase shift, respectively, in the two arms of QD-SOA MZI, α is the line width enhancement factor (LEF), $g_{1,2}$ is the SOA gain, and L is the active medium length. In order to evaluate the QD-SOA gain, we must use the theoretical model of the QD-SOA, which will be briefly discussed in Section 5.

5. The theoretical model of the QD-SOA

QD-SOA had been thoroughly investigated both theoretically and experimentally (see, for example, [15, 16] and references therein). The promising features of QD-SOA such as high saturation power, broad gain bandwidth, pattern-free amplification of single- and multi-channel signals, efficient WC can provide high-performance amplifiers and all-optical switches for optical networks [16].

QD is a nanostructure where the electron and hole movement is confined in the three dimensions, and these dimensions are of a few nanometers [15]. In QD, the charge carriers occupy only a restricted number of discrete energy levels like the electrons in an atom [15]. The density of states in QD is quantized, and the number of carriers necessary to fill these states decreases as compared to the structures with higher dimensionality. Consequently, the threshold current density in QD lasers substantially reduces, while the transparency and the population inversion necessary for the optical gain can be achieved more easily [15]. The QD grown by using the Stranski-Krastanov technology typically has a pyramidal shape with a base of about 15–20 nm and a height of about 5 nm [15]. The QD has a significant size dispersion, which results in the inhomogeneous broadening of the QD laser and SOA spectrum [15]. QD structures exhibit ultrafast gain recovery time which results in the ultrafast carrier dynamics [15]. The active layer of a QD-SOA contains one or several quantum wells (QW) referred to as a wetting layer (WL) with a continuous carrier energy band [15]. The electrons in the Stranski-Krastanov grown QD are typically characterized by two energy levels: the ground state (GS) situated about 100 meV below the band gap of WL and the excited state (ES), or the first excited level [15]. The energy level structure of a QD laser or QD-SOA is presented in **Figure 7**.

The carrier dynamics in QD is described by the system of the rate equations taking into account the following electron transitions: the fast electron transitions from WL to ES with the relaxation time $\tau_{wE} \sim 3$ ps; the fast electron transitions between ES and GS with the corresponding relaxation times $\tau_{EG} \approx 0.16$ ps; $\tau_{GE} \sim 1.2$ ps; the slow electron transitions from ES to WL with the escape time $\tau_{Ew} \sim 1$ ns. The QD-SOA rate equations have the form [12, 17]:
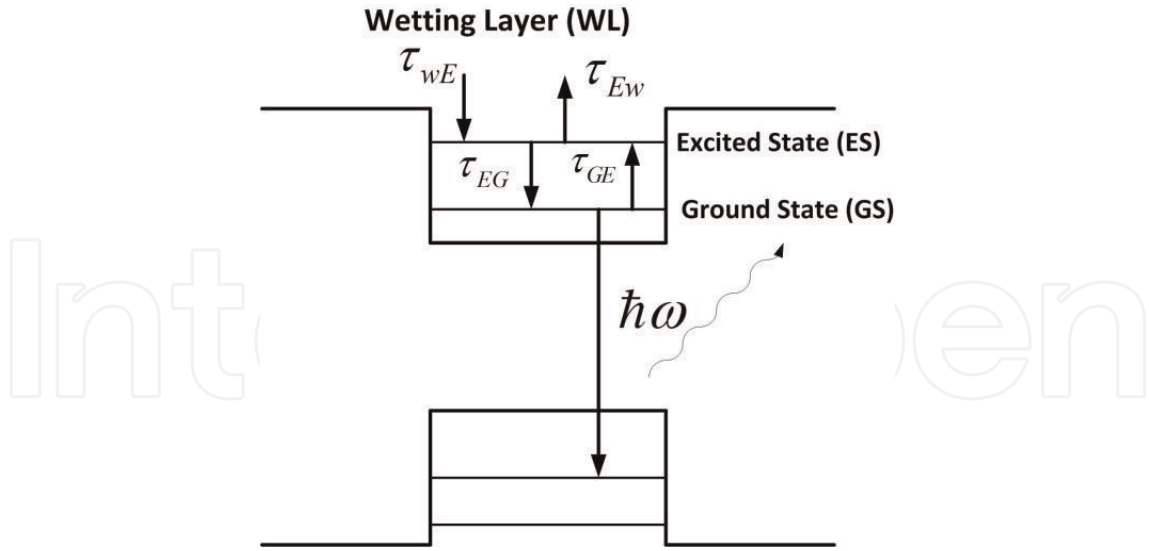
Figure 7. The energy level structure and the electron transitions in a QD.

$$\frac{\partial N_w}{\partial t} = \frac{J}{eL_w} - \frac{N_w(1-h)}{\tau_{wE}} + \frac{N_w}{\tau_{Ew}} - \frac{N_w}{\tau_{wR}} \tag{5}$$

$$\frac{\partial h}{\partial t} = \frac{N_w L_w (1-h)}{N_Q \tau_{wE}} - \frac{N_w L_w h}{N_Q \tau_{Ew}} - \frac{(1-f)h}{\tau_{EG}} + \frac{f(1-h)}{\tau_{GE}} \tag{6}$$

$$\frac{\partial f}{\partial t} = \frac{(1-f)h}{\tau_{EG}} - \frac{f(1-h)}{\tau_{GE}} - \frac{f^2}{\tau_R} - \frac{g_p L}{N_Q}(2f-1)S_p \frac{c}{\sqrt{\varepsilon_r}}$$
$$- \frac{g_s L}{N_Q}(2f-1)S_s \frac{c}{\sqrt{\varepsilon_r}} \tag{7}$$

where J is injection current density, N_w is the WL carrier density per unit volume, f is the electron occupation probability of GS, h is the electron occupation probability of ES, $S_{p,s}$ are the pump (data A or data B) and signal (clock stream) wave photon densities averaged over the length of SOA L, $g_{p,s}$ are the pump and signal wave modal gains, respectively, e is the electron charge, $N_Q \sim (10^{10} - 10^{12})$ cm^{-2} is the QD density per unit area, L_w is the effective thickness of the active layer, ε_r is the SOA material permittivity, and c is the free space light velocity. The average photon densities $S_{p,s}$ are given by Ben Ezra [12]:

$$S_{p,s}(\tau) = \frac{[S_{p,s}(\tau)]_{in}}{L} \int_0^L dz \exp\left(\int_0^z (g_{p,s} - \alpha_{int})dz'\right) \tag{8}$$

where $\tau = t - \left(\frac{z}{v_g}\right)$, t, z, v_g are time, coordinate, and the optical wave group velocity, respectively. The pump and signal wave phase $\varnothing_{p,s}$ and modal gain $g_{p,s}$ are given by, respectively [12]:

$$\theta_{p,s}(\tau) = -\frac{\alpha}{2} \int_0^L g_{p,s} dz \tag{9}$$

$$g_{p,s}(\omega) = \frac{2\Gamma N_Q}{a} \int d\omega F(\omega)\sigma(\omega_0)(2f-1) \tag{10}$$

where Γ is the confinement factor, l is the number of QD layers, a is the mean size of QD, $\sigma(\omega_0)$ is the cross section of interaction of photons of frequency ω_0 with carriers in QD at the transition frequency ω including the homogeneous broadening factor, $F(\omega)$ is the Gaussian distribution of the transition frequency in the QD ensemble related to the inhomogeneous broadening. The inhomogeneous broadening is caused by the QD shape and size variations as it was mentioned above. It is given by Ben Ezra [12]:

$$F(\omega) = \frac{1}{\Delta\omega\sqrt{\pi}} \exp\left[-\frac{(\omega-\overline{\omega})^2}{(\Delta\omega)^2}\right] \tag{11}$$

where $\Delta\omega$ is related to the inhomogeneous bandwidth, $\gamma_{inhom} = 2\Delta\omega\sqrt{ln2}$, and $\overline{\omega}$ is the average transition frequency.
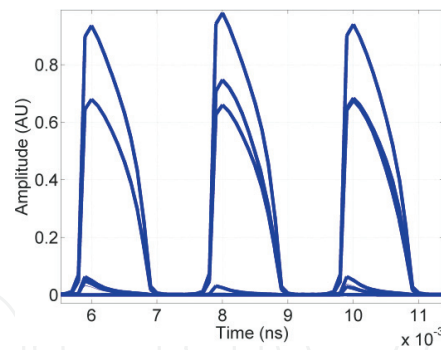
6. The simulation results

We solved numerically Eqs. (3)–(11) for the typical values of parameters [12] for the QD-SOA–based all-optical loop shown in **Figure 6** [6]. The numerical simulations have been carried out for the OOK and pulse amplitude modulation 4 (4-PAM) formats [6]. We used the MATLAB environment. Simulation results for the eye diagrams in the case of the OOK modulation format are shown in **Figures 8** and **9**.

We used the QD-SOA–based all-optical memory model with the loop length of L = 2 km and the input OOK modulated signal with the bit rate of 50 Gb/s and the quality factor at the input Q = 15.8932. The comparison of the eye diagrams presented in **Figures 8** and **9** shows that after 4 rounds in the loop, the quality factor of the signal decreases by approximately 18%.
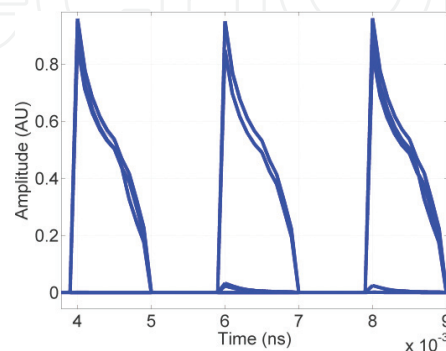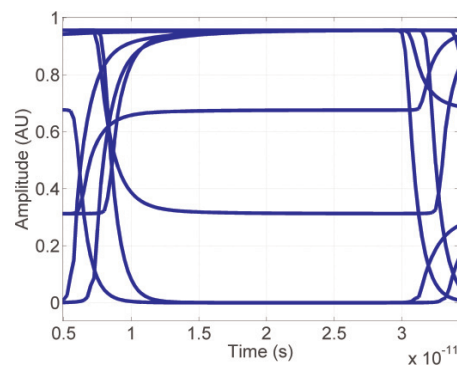

Figure 8. The eye diagram for the OOK modulation format, a bit rate of 50 Gb/s after one round in the QD-SOA–based all-optical memory loop. The memory loop length L = 2 km, T = 10 μs, the quality factor Q = 13.3156.
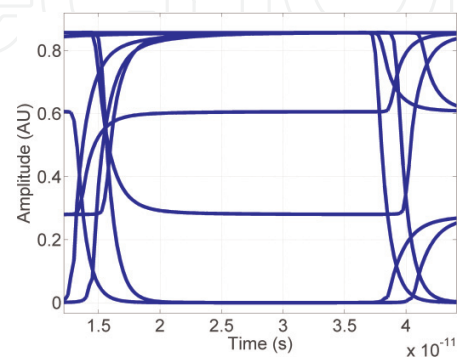
Figure 9. The eye diagram for the OOK modulation format, a bit rate of 50 Gb/s after four rounds in the QD-SOA–based all-optical memory loop. The memory loop length L = 2 km, T = 40 µs, the quality factor Q = 13.0327.

The simulations results for the 4-PAM modulation format, QD SOA–based all-optical memory loop with the length of L = 1 km and bit rates of 50 and 100 Gb/s are shown in **Figures 10–13**, respectively.

Eye diagrams in **Figures 10** and **11** clearly show that for the bit rate of 50 Gb/s, the patterning effect is negligible after two rounds in the memory loop. In the case of the bit rate of 100 Gb/s, the patterning effect is slightly pronounced after the two rounds in the memory loop as it is
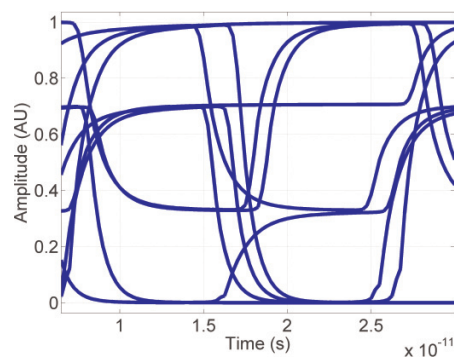

Figure 10. The eye diagram for 4-PAM modulation format and a bit rate of 50 Gb/s, the memory loop length L = 1 km. The signal is at the input of the all-optical memory loop.

Figure 11. The eye diagram for 4-PAM modulation format and a bit rate of 50 Gb/s, the memory loop length L = 1 km. The signal is after two rounds in the all-optical memory loop.
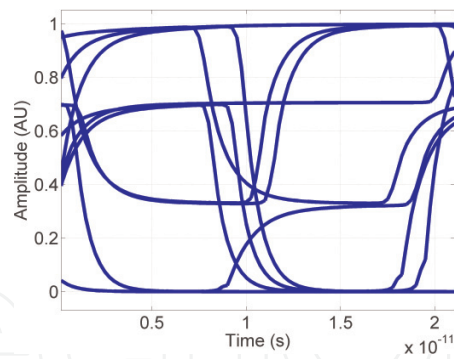
Figure 12. The eye diagram for 4-PAM modulation format and a bit rate of 100 Gb/s, the memory loop length L = 1 km. The signal is at the input of the all-optical memory loop.

Figure 13. The eye diagram for 4-PAM modulation format and a bit rate of 100 Gb/s, the memory loop length L = 1 km. The signal is after two rounds in the all-optical memory loop.

seen from **Figures 12** and **13**. The QD-SOA–based all-optical memory performance does not deteriorate up to the bit rate of 100 Gb/s.

The numerical estimations show that for loop length L = 1 km, the light velocity in the optical fiber $v \approx 2 \times 10^8$ m/s and the bit rates of 50 and 100 Gb/s the all-optical memory storage values are of 0.25 and 0.5 Mb, the storage times are 5 and 10 μs, respectively [6].

7. Conclusions

Optical signal processing substantially increases the device processing speed, provides an alternative to electronic techniques, and, at the same time, can enhance the processing capabilities of electronics when the optical and electronic signal processing techniques are combined. Optical packet-switched networks are promising candidates for the advanced optical telecommunication systems. All-optical signal processing is essential for ultrafast OPS in such networks. Flip-flop memory is a basic component of an all-optical packet switch. We discussed the all-optical memory based on SOA-MZI. It is characterized by the high performance due to the SOA high nonlinearity, low switching power, wide gain bandwidth, compact size, and integration capability with other photonic devices. Unfortunately, the SOA operation rate is limited by its comparatively slow gain recovery time.

We proposed a novel architecture of the ultrafast all-optical memory based on MZI with two QD-SOA. QD-SOA is characterized by high operation rate and low threshold current caused by the 3D carrier confinement and fast electron transitions in QD. For this reason, the operation rate of the proposed all-optical memory loop increases up to 100 Gb/s. The time delay in the typical push-pull scheme of the memory loop is replaced with the output signal phase difference caused by the signal power difference in the MZI arms due to the highly efficient XPM in QD-SOA. The DSP block is inserted for the dispersion and nonlinearity impairment mitigation. The proposed all-optical memory loop includes only one MZI with two QD-SOA and reduces the complexity of electronic synchronization scheme. We carried out numerical simulations of the proposed all-optical memory loop based on the QD-SOA rate equations and the expression for the MZI output power for the OOK and 4-PAMmodulation formats. The simulation results show that the proposed all-optical memory exhibits a high performance up to the bit rate of 100 Gb/s and the corresponding memory storage and storage time values of 0.5 Mb and 10 μs, respectively.

Author details

Yossef Ben Ezra[1,2] and Boris I. Lembrikov[1]*

*Address all correspondence to: borisle@hit.ac.il

1 Department of Electrical Engineering and Electronics, Holon Institute of Technology (HIT), Holon, Israel

2 MER Cellos, Holon, Israel

References

[1]   Agrell E, Karlsson M, Chraplyvy AR, et al. Roadmap of optical communications. Journal of Optics. 2016;**18**:1–40. DOI: 10.1088/2040-8978/18/6/063002

[2]   Willner AE, Khaleghi S,Chitgarha MR, Yilmaz OF. All-optical signal processing. Journal of Lightwave Technology. 2014;**32**:660–680. DOI: 10.1109/JLT.2013.2287219

[3]   Agrawal GP. Fiber-Optic Communication Systems. 4th ed. New York: Wiley; 2010. ISBN: 978-0-470-50511-3

[4]   Agrawal GP. Nonlinear Fiber Optics. 5th ed. New York: Academic Press; 2013. ISBN: 978-0-12397-023-7

[5]   Liu Y, Hill MT, Calabretta N, Tangdiongga E, Geldenhuys R, Zhang S, Li Z, De Waardt H, Khoe GD, Dorren HJS. All-optical signal processing for optical packet switching networks. In: Proceedings of SPIE; September 15, 2005; San Diego, California, USA; 2005. 59070J-1-12. DOI: 10.1117/12.621346

[6] Ben Ezra Y, Lembrikov BI. All-optical memory based on quantum dot semiconductor optical amplifiers (QD-SOAs) for advanced modulation formats. In: Proceedings of 18th International Conference on Transparent Optical Networks (ICTON 2016); July 10-14, 2016; Trento, Italy; Tu. A5.3 1-3. ISBN: 978-1-5090-1466-8

[7] Dorren HJS, Hill MT, Liu Y, Calabretta N, Srivatsa A, Huijskens FM, De Waardt H, Khoe GD. Optical packet switching and buffering by using all-optical signal processing methods. Journal of Lightwave Technology. 2003;**21**:2–12. DOI: 10.1109/JLT.2002.803062

[8] Xuelin Y, Qiwei W, Weisheng H. High-speed all-optical long-term memory using SOA MZIs: Simulation and experiment. Optics Communications. 2012;**285**:4043-4047. DOI: 10.1016/j.optcom.2012.06.027

[9] Singh P, Tripathi D Kr, Jaiswal S, Dixit HK. All-optical logic gates: Designs, classification and comparison. Advances in Optical Technologies. 2014;**2014**:1–13. DOI: 10.1155/2014/275083

[10] Shehata MI, Mohammed NA. Design and optimization of novel two inputs logic gates (NOT, AND, OR and NOR) based on single commercial TW-SOA operating at 40 Gbit/s. Optical and Quantum Electronics. 2016;**48**:336(1–16). DOI: 10.1007/s1 1082-016-0602-2

[11] Stubkjaer KE. Semiconductor optical amplifier-based all-optical gates for high-speed optical processing. IEEE Journal of Selected Topics in Quantum Electronics. 2000;**6**:1428–1435. DOI: 10.1109/2944.902198

[12] Ben Ezra Y, Lembrikov BI, Haridim M. Ultra-fast all-optical processor based on quantum dot semiconductor optical amplifiers (QD-SOA). IEEE Journal of Quantum Electronics. 2009;**45**:34-41. DOI: 10.1109/JQE.2008.2003497

[13] Sun H, Wang Q, Dong H, Dutta NK. XOR performance of a quantum dot semiconductor optical amplifier based Mach-Zender interferometer. Optics Express. 2005;**13**:1892-1899. ISSN: 1094-4087

[14] Wang Q, Zhu G, Chen H, Jaques J, Leuthold J, Picirilli AB, Dutta NK. Study of all-optical XOR using Mach-Zender interferometer and differential scheme. IEEE Journal of Quantum Electronics. 2004;**40**:703-710. DOI: 10.1109/JQE.2004.828261

[15] Rafailov EU, Cataluna MA, Avrutin EA. Ultrafast Lasers Based on Quantum Dot Structures. Weinheim: Wiley-VCH; 2011. p. 250. ISBN: 978-3-527-40928-0

[16] Sugawara M, Ebe H, Hatori N, et al. Theory of optical signal amplification and processing by quantum-dot semiconductor optical amplifiers. Physical Review B. 2004;**69**:235332-1-2 35332-39. DOI: 10.1103/PhysRevB.69.235332

[17] Qasaimeh O. Optical gain and saturation characteristics of quantum-dot semiconductor optical amplifiers. IEEE Journal of Quantum Electronics. 2003;**39**:793-798. DOI: 10.1109/JQE.2003.810770